Supporting Information for

A novel stalactiform structural CoNi-rGO for supercapacitors with enhanced electrochemical performance

Yang Sun,‡[b] Zhaoyi Zhang,‡[a] Cong Xiang,[a] Yifan Jiang,[a] Yan Feng,[a] Xiaomei Cheng,[a] Xiangzi Li,*[a] and Meifang Wang *[a]

[a] *Department of Pharmacy, Wannan Medical College, Wuhu 241002, China*

[b] *School of Chemical and Environmental Engineering, Anhui Polytechnic University, Wuhu, 241000, China*

* Corresponding authors.

E-mail addresses: li-xiang-zi@163.com *(X. Z. Li),* zijingyuwinter@163.com *(M. F. Wang).*

S1 Experiment Characterization

The X-ray powder diffraction (XRD, MiniFlex600) was conducted on a D/teX Ultra2 diffractometer. Field emission scanning electron microscopy (FESEM) images were obtained on a Hitachi S-4800 field emission scanning electron microscope with an operating voltage of 5 kV. Transmission electron microscopy (TEM) and HAADF-STEM-EDX mapping images were obtained on a Hitachi HT7700 transmission electron microscope, employing an accelerating voltage of 120 kV. X-ray photoelectron spectroscopy (XPS) of the product was carried out using a Thermo ESCALAB 250 instrument, employing monochromic Al Kα (hν = 1486.6 eV) at a power of 150 W. Nitrogen adsorption-desorption isotherms were measured at the liquid nitrogen temperature (77 K), using a Micromeritics ASAP 2460 analyzer. Surface areas were calculated by the Brunauer-Emmett-Teller (BET) method. Operando Raman measurements were recorded using a Raman spectrometer (RENISHAW in Via system, U.K.) with a 532 nm He/Ne laser as the excitation source.

S2 Electrochemical Measurements

The electrochemical performance measurements were carried out by CHI 660E electrochemical workstation (Chenhua Instruments, China). In a three-electrode system, the samples were adopted directly as the working electrodes (1×1 cm^2), Hg/HgO and Pt wires as reference and counter electrodes, respectively. Cyclic voltammetry (CV, 0 - 0.7 V), electrochemical impedance spectroscopy (EIS, at open circuit potential with an amplitude of 5 mV, 10^5 - 0.01 Hz) and galvanostatic charge/discharge (GCD, 0 - 0.5 V) measurements were examined in 2 M KOH aqueous electrolytes. At different current densities, the specific gravimetric capacitance (C_s, or F g^{-1}) of the hybrid battery was calculated by equation (S1): [1]

$$C_s = \frac{i * \triangle T}{m * \triangle V} \tag{S1}$$

where m (g) is the mass of the active material, i (A) is the constant discharging current, ΔT (s) is the duration of the discharge process and ΔV (V) is the voltage window.

An asymmetric supercapacitor (ASC) was prepared using S-CoNi-rGO as the positive electrode, the activated carbon (AC) as the negative electrode, and glass fiber paper as the separator. The electrochemical test was carried out in 2 M KOH electrolyte. The AC electrode was made by mixing active materials, acetylene black and polyvinylidene fluoride with a mass ratio of 7:2:1 on a nickel foam and then drying at 60 °C for 24 h.

The charge balance of the supercapacitor follows $q^+ = q^-$, where q^+ and q^- represent the charges stored by the positive and negative electrodes respectively. The optimized mass ratio between the positive and negative electrode materials for S-CoNi-rGO//AC can be calculated based on the charge balance relationship ($q^+ = q^-$) in the following equation: [2,3]

$$\frac{m^+}{m^-} = \frac{C^- \Delta V^-}{C^+ \Delta V^+} \qquad \text{(S2)}$$

where $C^{+/-}$ (F g^{-1}) are the specific capacitances of positive and negative electrodes, $\Delta V^{+/-}$ (V) are the potential windows of positive and negative electrodes, and $m^{+/-}$ (g) stands for the loading masses of materials on the positive and negative electrodes.

The energy density (E, Wh kg^{-1}) and power density (P, kW kg^{-1}) were obtained from GCD curves according to the following formula: [4]

$$E = \frac{C_S \Delta V^2}{7.2} \qquad \text{(S3)}$$

$$P = \frac{3600E}{\Delta t} \qquad \text{(S4)}$$

where C_S (F g^{-1}) represents the specific capacitance, ΔV (V) stands for the potential window, Δt (s) stands for the time of discharging, respectively.

S3 Supplementary Tables and Figures

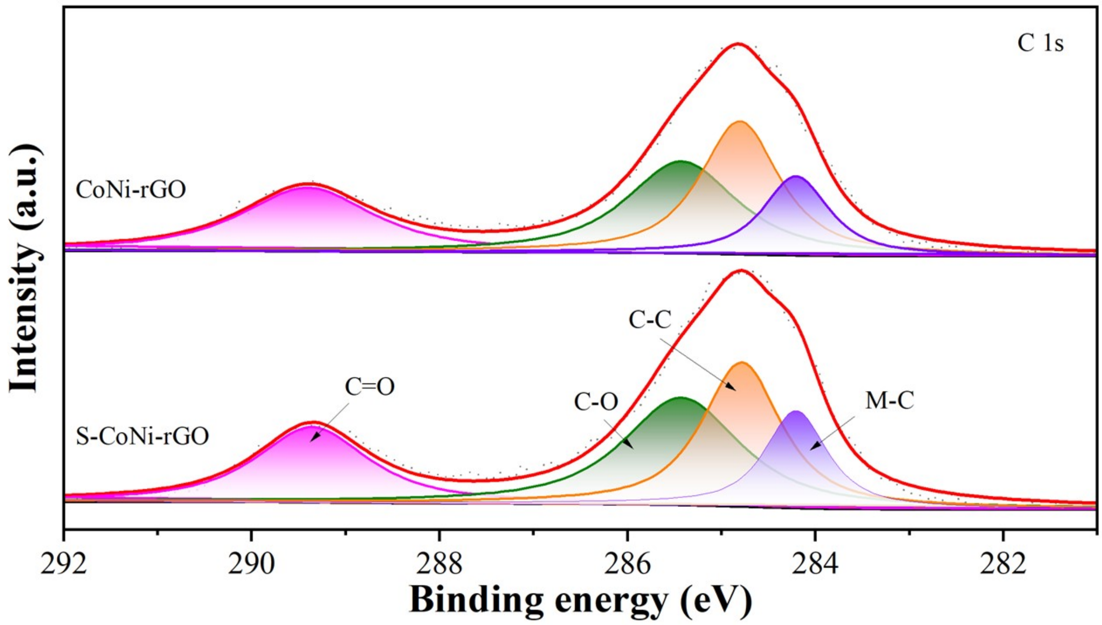

Fig. S1. XPS spectra of CoNi-rGO, S-CoNi-rGO for C 1s.

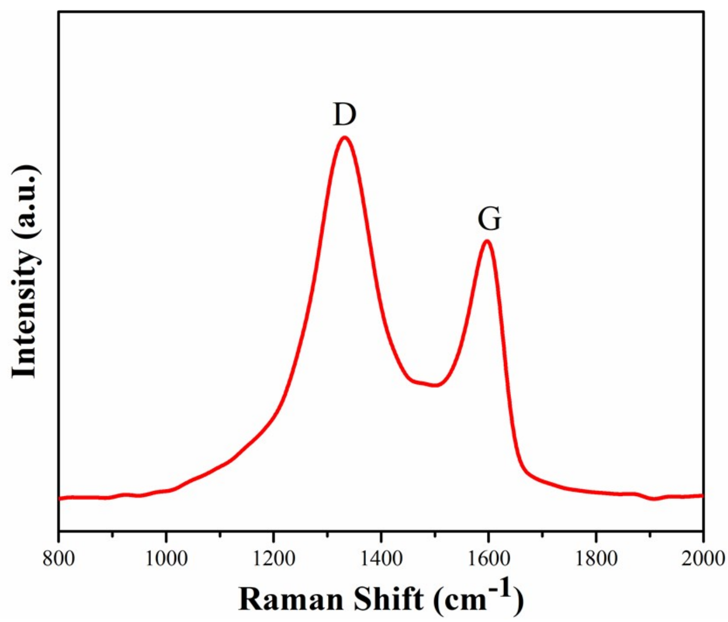

Fig. S2. Raman spectra of S-CoNi-rGO.

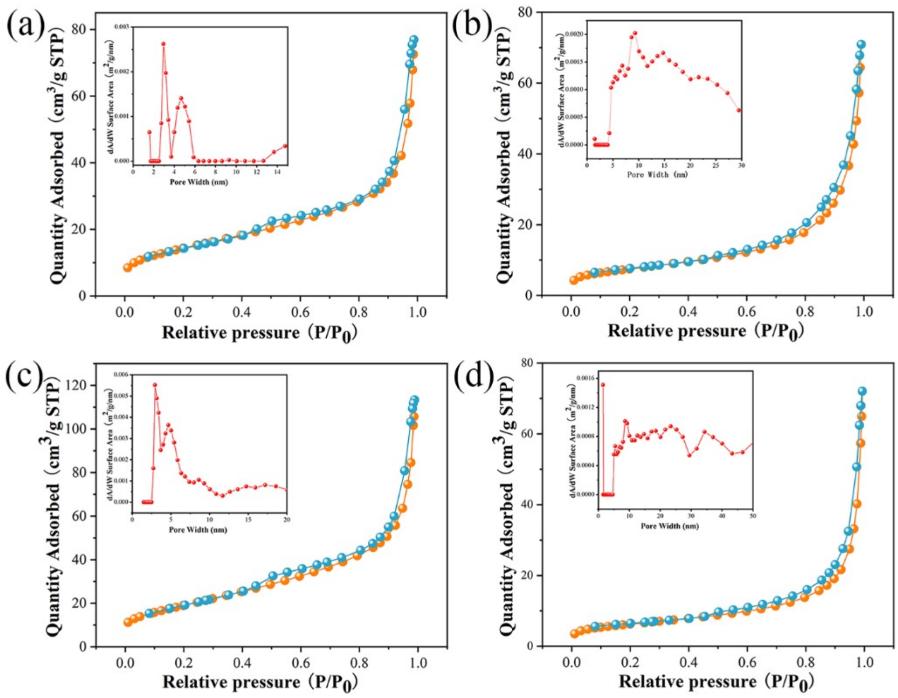

Fig. S3. N_2 adsorption/desorption isotherms and pore-size (inset) distributions of (a) CoNi-1, (b) CoNi-F, (c) CoNi-rGO, (d) S-CoNi-rGO, respectively.

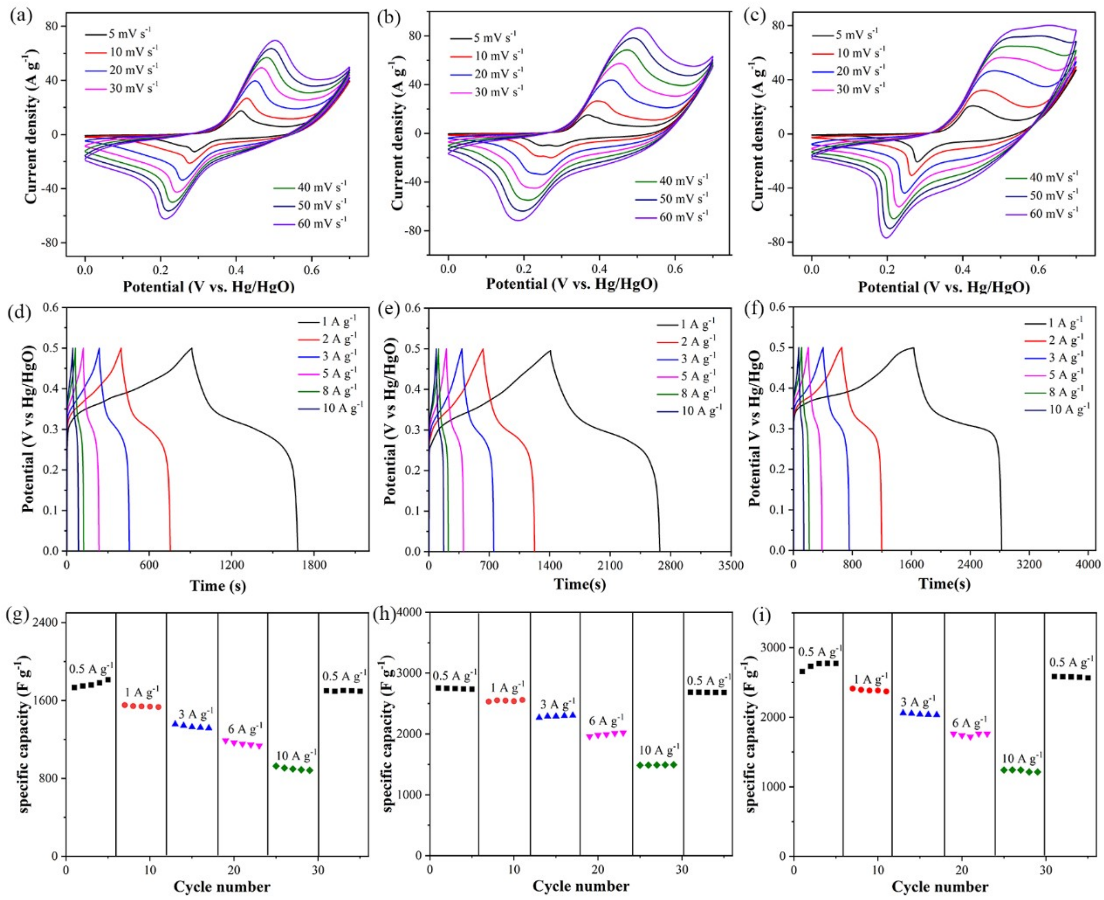

Fig. S4. (a-c) CV curves at different scan rates, (d-f) GCD curves at different current densities, (g-i) the cycling performance at various current densities of CoNi-1, CoNi-F, CoNi-rGO.

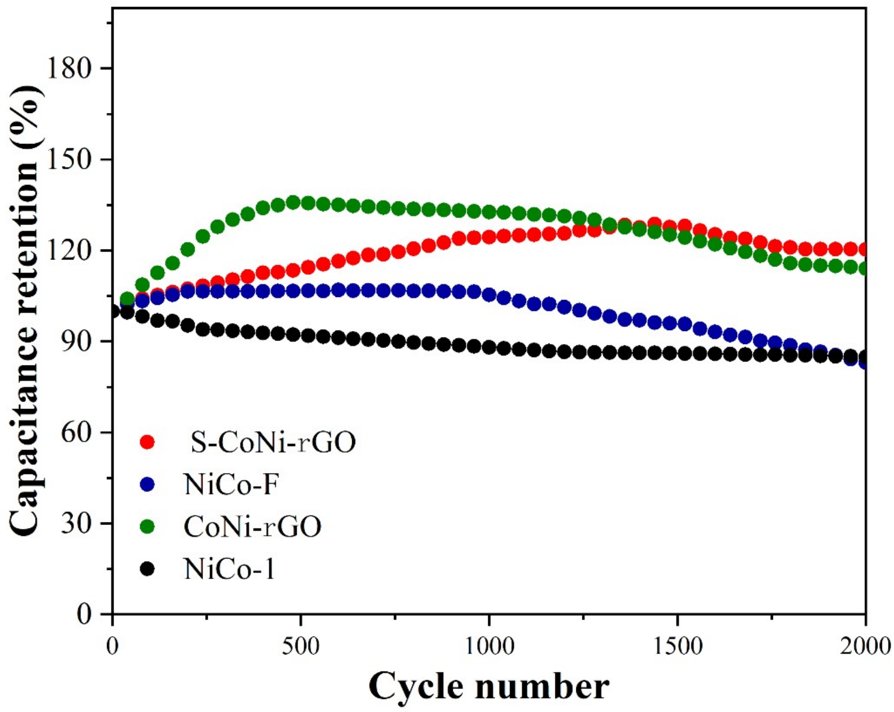

Fig. S5. The cycling stability for CoNi-1, CoNi-F, CoNi-rGO and S-CoNi-rGO at current density of 10 A g^{-1}.

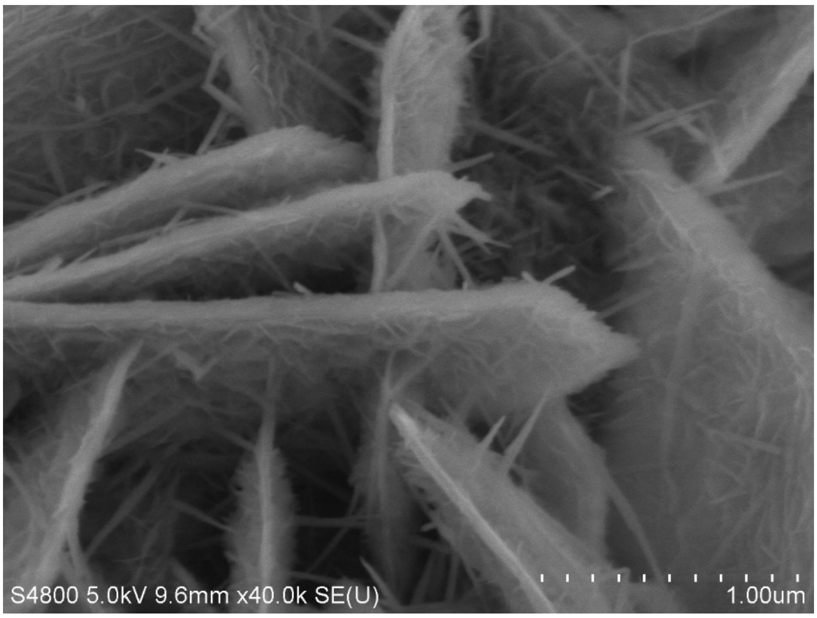

Fig. S6. The SEM images of S-CoNi-rGO after 10000 recycles tests.

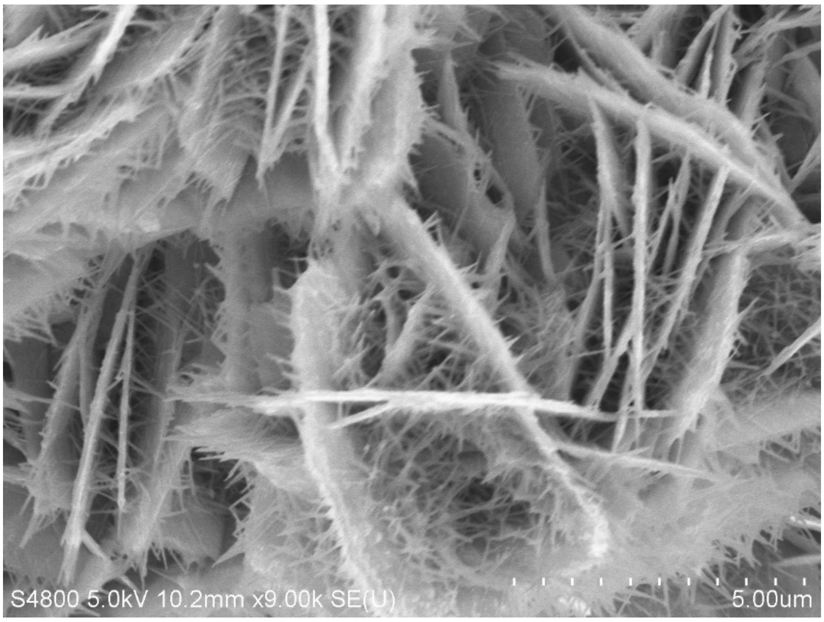

Fig. S7. The SEM images of S-CoNi-rGO // AC ASC device after 5000 recycles tests.

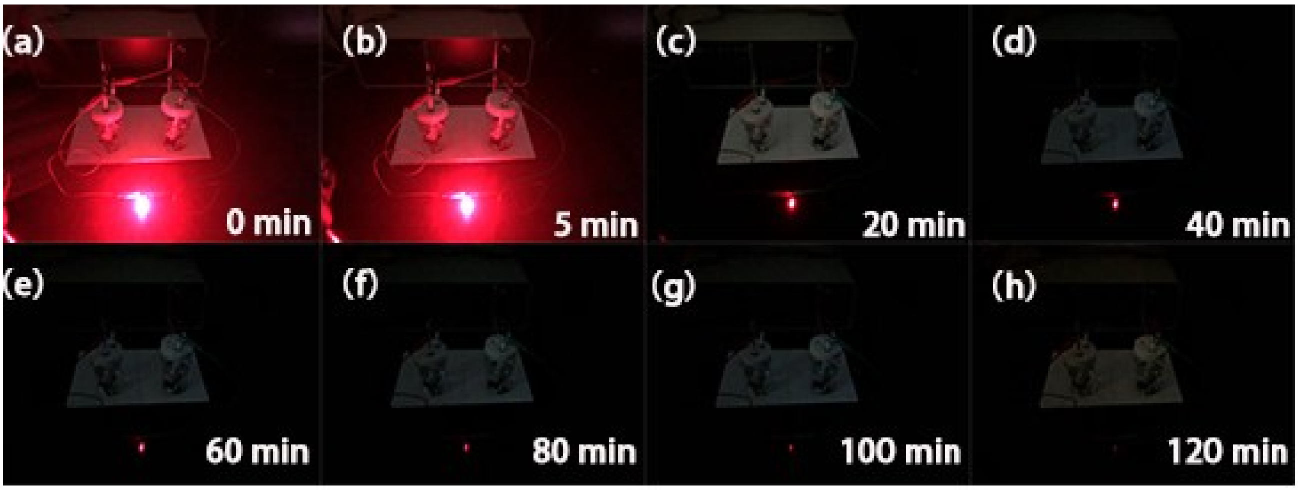

Fig. S8. (a-h) LED-driven tests during 120 min.

Table S1. The specific surface area and pore volume of of CoNi-1, CoNi-F, CoNi-rGO, S-CoNi-rGO.

Materials	CoNi-1	CoNi-F	CoNi-rGO	S-CoNi-rGO
Specific surface area ($m^2\ g^{-1}$)	51.94	26.88	69.59	32.52
Pore volume ($cm^3\ g^{-1}$)	0.119	0.110	0.175	0.132

Table S2. Comparison of S-CoNi-rGO//AC device electrochemical performances with those reported literatures.

Hybrid battery	Electrolyte	Energy density W h kg^{-1}	Power density kW kg^{-1}	Ref.
Co_3O_4@$Ni(OH)_2$ //AC	PVA:KOH	40.0	3.45	[5]
NiCo-MOF//AC	PVA:KOH	45.3	0.85	[4]
$NiCo_2O_4$@$Ni(OH)_2$//AC	2M KOH	98.5	0.85	[6]
CuCo HNSs/NF//AC	1M KOH	144.4	40	[7]
CF@CuO@CoNi LDH//RGO	2M KOH	92.5	0.4	[8]
$Ni(OH)_2$/CNT//AC	3M KOH	32.5	1.8	[9]
$NiCo_2S_4$@$Ni(OH)_2$//AC	2M KOH	53.3	0.29	[10]
$Co(OH)_2$/fCNT‖fCNT	PVA:KOH	17	7	[11]
NMCOH-2.4//NDG	3 M KOH	92	1.7	[12]
S-CoNi-rGO //AC	2 M KOH	114.03	0.85	This work

Table S3. S-CoNi-rGO//AC device electrochemical performances at different current densities.

Hybrid battery	The current density A g^{-1}	The capacitance F g^{-1}	Energy density Wh kg^{-1}	Power density kW kg^{-1}
S-CoNi-rGO//AC	1	284.1	114.03	0.854
S-CoNi-rGO//AC	2	276.9	111.14	1.724
S-CoNi-rGO//AC	3	267.9	107.53	2.579
S-CoNi-rGO//AC	4	259.2	104.04	3.419

S-CoNi-rGO//AC	5	253.5	101.75	4.249
S-CoNi-rGO//AC	8	246.0	96.57	6.803
S-CoNi-rGO//AC	10	234.7	94.21	8.501

Supplementary References

[1] A. Gowrisankar, T. Selvaraju, *Langmuir*, 2021, **37**, 5964-5978.

[2] D. Merum, R. R. Nallapureddy, M. R. Pallavolu, T. K. Mandal, R. R. Gutturu, N. Parvin, A. N. Banerjee and S. W. Joo, *ACS Appl. Energy Mater*., 2022, **5**, 5561-5578.

[3] J. J. Xia, L. M. Zhang, S. G. Xuan, Y. H. Ni, L. Zhang, *CrystEngComm*, 2022, **24**, 2159-2170.

[4] H. Li, X. F. Wang, L. L. Dai, F. J. Guo, H. Y. Mi, C. C. Ji and L.Y. Sun, *Inorg. Chem*., 2022, **61**, 3866-3874.

[5] X. Bai, Q. Liu, J. Liu, H. Zhang, Z. Li, X. Jing, P. Liu, J. Wang and R. Li, *Chem. Eng. J.*, 2017, **31**, 35-45.

[6] P. Xia, Q. Y. Wang, Y. T. Wang, W. Quan, D. L. Jiang and M. Chen, *J. Alloy. Compd.*, 2019, **771**, 784-792.

[7] N. Jayababu, D. Kim, *Small*, 2021, **17**, 2102369.

[8] F. Chen, C. Chen, Q. Hu, B. Xiang, T. T. Song, X. F. Zou, W. N. Li, B. X. Xiong and M. S. Deng, *Chem. Eng. J.*, 2020, **401**, 126145.

[9] B. Guan, Y. Li, B. Yin, K. Liu, D. Wang, H. Zhang and C. Cheng, *Chem. Eng. J.*, 2017, **308**, 1165-1173.

[10] Y. Yang, D. Cheng, S. Chen, Y. Guan and J. Xiong, *Electrochim. Acta*, 2016, **193**, 116-127.

[11] R. Ranjithkumar, S. E. Arasi, P. Devendran, N. Nallamuthu, A. Arivarasan, P. Lakshmanan, S. Sudhahar and M. K. Kumar, *Diam. Relat. Mater.*, 2020, **110**, 108120.

[12] F. N. I. Sari, K. C. Lin and J. M. Ting, *Appl. Surf. Sci.*, 2022, **576**, 151805.